Chapter 10: Global Climate Projections

Coordinating Lead Authors: Gerald A. Meehl, Thomas F. Stocker

Lead Authors: William Collins, Pierre Friedlingstein, Amadou Gaye, Jonathan Gregory, Akio Kitoh, Reto Knutti, James Murphy, Akira Noda, Sarah Raper, Ian Watterson, Andrew Weaver, Zong-Ci Zhao

Contributing Authors: J. Annan, J. Arblaster, C. Bitz, A. le Brocq, P. Brockmann, V. Brovkin, L. Buja, P. Cadule, G. Clarke, M. Collier, M. Collins, E. Driesschaert, N.A. Diansky, M. Dix, K. Dixon, J.-L. Dufresne, M. Dyurgerov, M. Eby, N. Edwards, S. Emori, P. Forster, R. Furrer, J. Hansen, G. Hegerl, M. Holland, A. Hu, P. Huybrechts, C. Jones, F. Joos, J. Jungclaus, J. Kettleborough, M. Kimoto, T. Knutson, M. Krynytzky, D. Lawrence, M.-F. Loutre, J. Lowe, D. Matthews, M. Meinshausen, S. Müller, S. Nawrath, J. Oerlemans, M. Oppenheimer, J. Overpeck, T. Palmer, A. Payne, G.-K. Plattner, J. Räisänen, E. Roeckner, G.L. Russell, A. Rinke , D. Salas y Melia, G. Schmidt, A. Schmittner, B. Schneider, A. Shepherd, A. Sokolov, D. Stainforth, P. Stott, R. Stouffer, K. Taylor, C. Tebaldi, H. Teng, L. Terray, D. Vaughan, E. M. Volodin, B. Wang, T. M. L. Wigley, M. Wild, R. van de Wal, J. Yoshimura, Y. Yu, S. Yukimoto

Review Editors: Myles Allen, Govind Ballabh Pant

Date of Draft: 3 March 2006

Notes: TSU compiled version

Figures

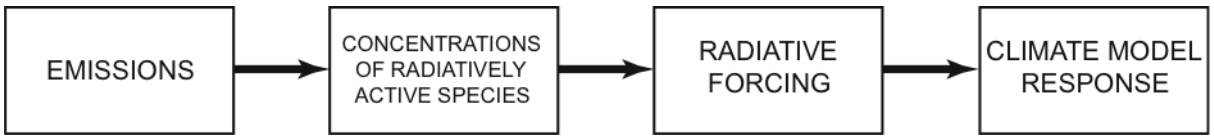

Figure 10.1.1. Contributions to uncertainty in climate model projections.

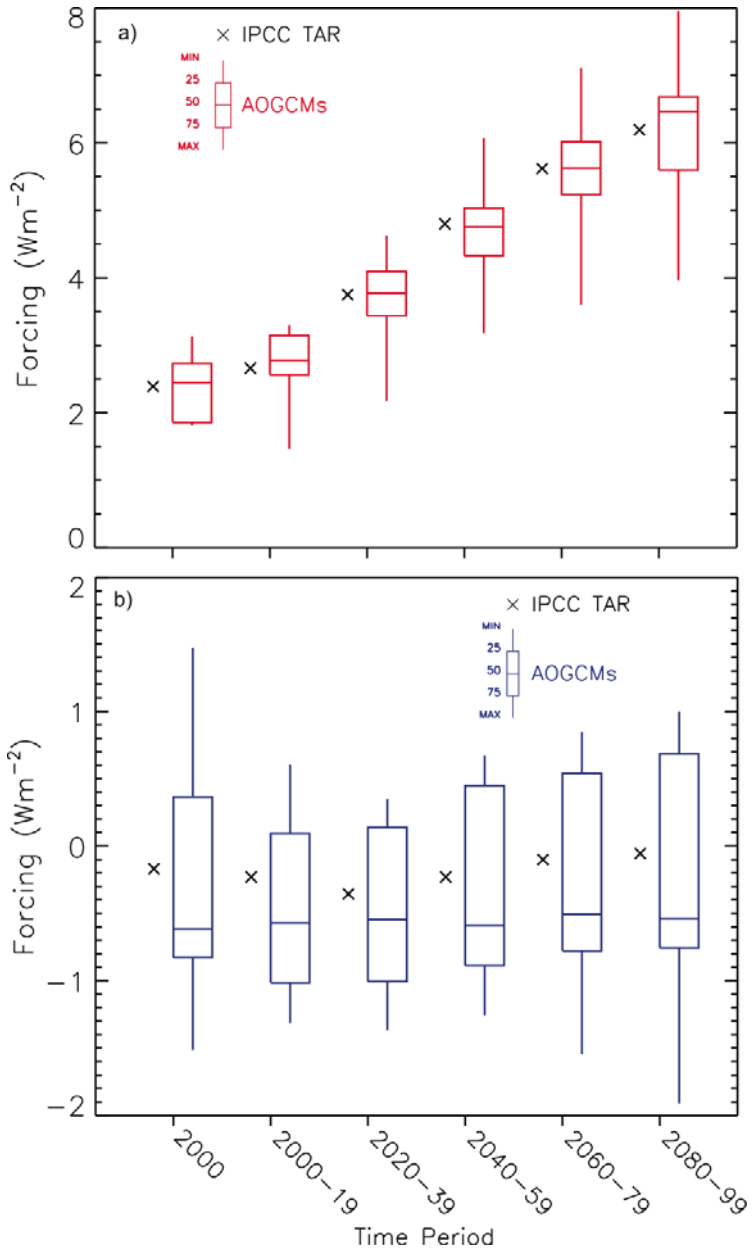

Figure 10.2.1. Radiative forcings for the period 2000–2100 for the SRES A1B scenario diagnosed from AOGCMs and from the IPCC TAR (2001) forcing formulas (Forster and Taylor, 2006). a) longwave forcing; b) shortwave forcing. The AOGCM results are plotted with box-and-whisker diagrams representing percentiles of forcings computed from 14 models in the AR4 multi-model ensemble. The centerline within each box represents the median value of the model ensemble. The top and bottom of each box shows the 25th and 75th percentiles, and the top and bottom of each whisker displays the minimum and maximum values in the ensemble, respectively. The AOGCM forcings are computed relative to the starting times of the individual integrations in the 19th century. The IPCC TAR forcings are computed relative to 1850. Note: a list of the models used for this and each of the following multi model figures will be given for the final draft.

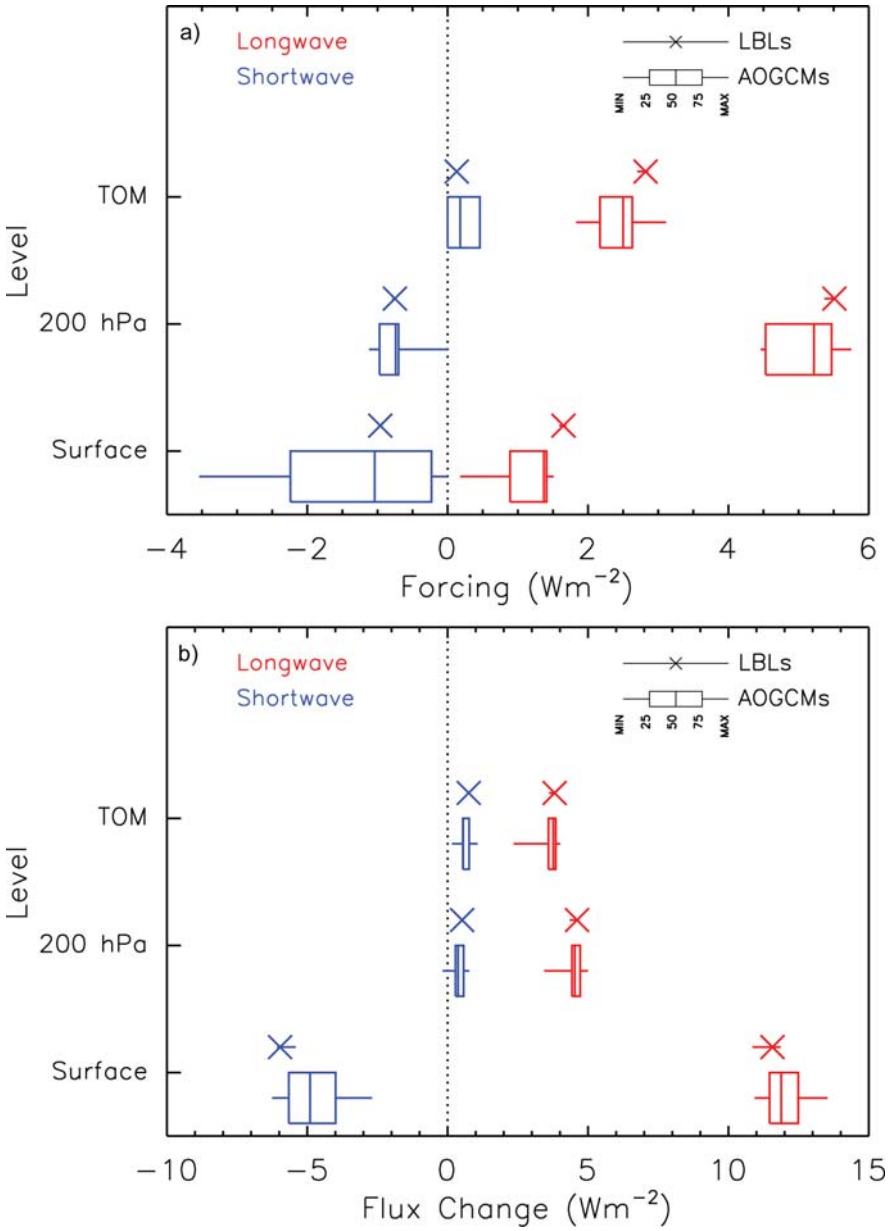

Figure 10.2.2. Comparison of shortwave and longwave instantaneous radiative forcings and flux changes computed from AOGCMs and line-by-line (LBL) radiative transfer codes (Collins et al., 2006b). a) instantaneous forcing from doubling CO_2 from its concentration in 1860; b) changes in radiative fluxes caused by the 20% increase in H_2O expected in the climate produced from doubling CO_2. The forcings and flux changes are computed for clear-sky conditions in mid-latitude summer and do not include effects of stratospheric adjustment. No other well-mixed greenhouse gases are included. The minimum-to-maximum range and median are plotted for five representative LBL codes. The AOGCM results are plotted with box-and-whisker diagrams (see caption for Figure 10.2.1) representing percentiles of forcings from 20 models in the AR4 multi-model ensemble.

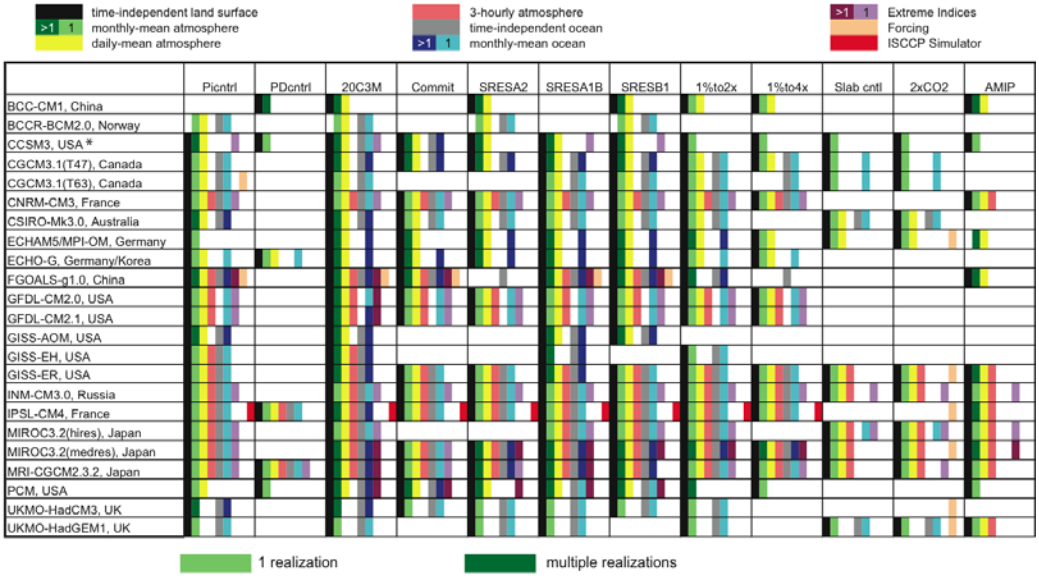

	Picntrl	PDcntrl	20C3M	Commit	SRESA2	SRESA1B	SRESB1	1%to2x	1%to4x	Slabcntl	2xCO2	AMIP
BCC-CM1, China		2	4		2		2	1	1			4
BCCR-BCM2.0, Norway	1		1		1		1					
CCSM3, USA *	2	1	9	5	5	7	8	1	1	1	1	1
CGCM3.1(T47), Canada	1		5	5	5	5	4	1	1	1	1	
CGCM3.1(T63), Canada	1		1			1	1	1		1	1	
CNRM-CM3, France	1		1	1	1	1	1	1	1			1
CSIRO-Mk3.0, Australia	2		3	1	1	1	1	1		1	1	
ECHAM5/MPI-OM, Germany	1		3	3	3	3	3	3	1	1	1	3
ECHO-G, Germany/Korea	1	1	5	4	3	3	3	1	1			
FGOALS-g1.0, China	3		3	3		3	3	3				3
GFDL-CM2.0, USA	1		3	1	1	1	1	1	1			
GFDL-CM2.1, USA	1		3	1	1	1	1	1	1			
GISS-AOM, USA	2		2			2	2					
GISS-EH, USA	1		5			4		1				
GISS-ER, USA	1		9	1	1	5	1	1	1	1	1	4
INM-CM3.0, Russia	1		1	1	1	1	1	1	1	1	1	1
IPSL-CM4, France	1	1	2	1	1	1	1	1	1			6
MIROC3.2(hires), Japan	1		1			1	1	1		1	1	1
MIROC3.2(medres), Japan	1		3	1	3	3	3	3	3	1	1	3
MRI-CGCM2.3.2, Japan	1	1	5	1	5	5	5	1	1	1	1	1
PCM, USA	1	1	4	3	4	4	4	5	1			1
UKMO-HadCM3, UK	2		2	1	1	1	1	1				
UKMO-HadGEM1, UK	1		1		1	1		1		1	1	1

Table 10.3.1. a) Summary of climate change model experiments performed with AOGCMs. Coloured fields indicate that some but not necessarily all variables of the specific data type (separated by climate system component and time interval) have been archived at PCMDI to be used in this report. Where different color shadings are given in the legend, the colour indicates whether single or multiple ensemble members are available; b) number of ensemble members performed for each experiment and each scenario. Details on the scenarios, variables and models can be found at the PCMDI webpage (http://www-pcmdi.llnl.gov/ipcc/about_ipcc.php). Status: February 2006.
* Some of the ensemble members using the CCSM3 were run on the Earth Simulator in Japan in collaboration with CRIEPI.

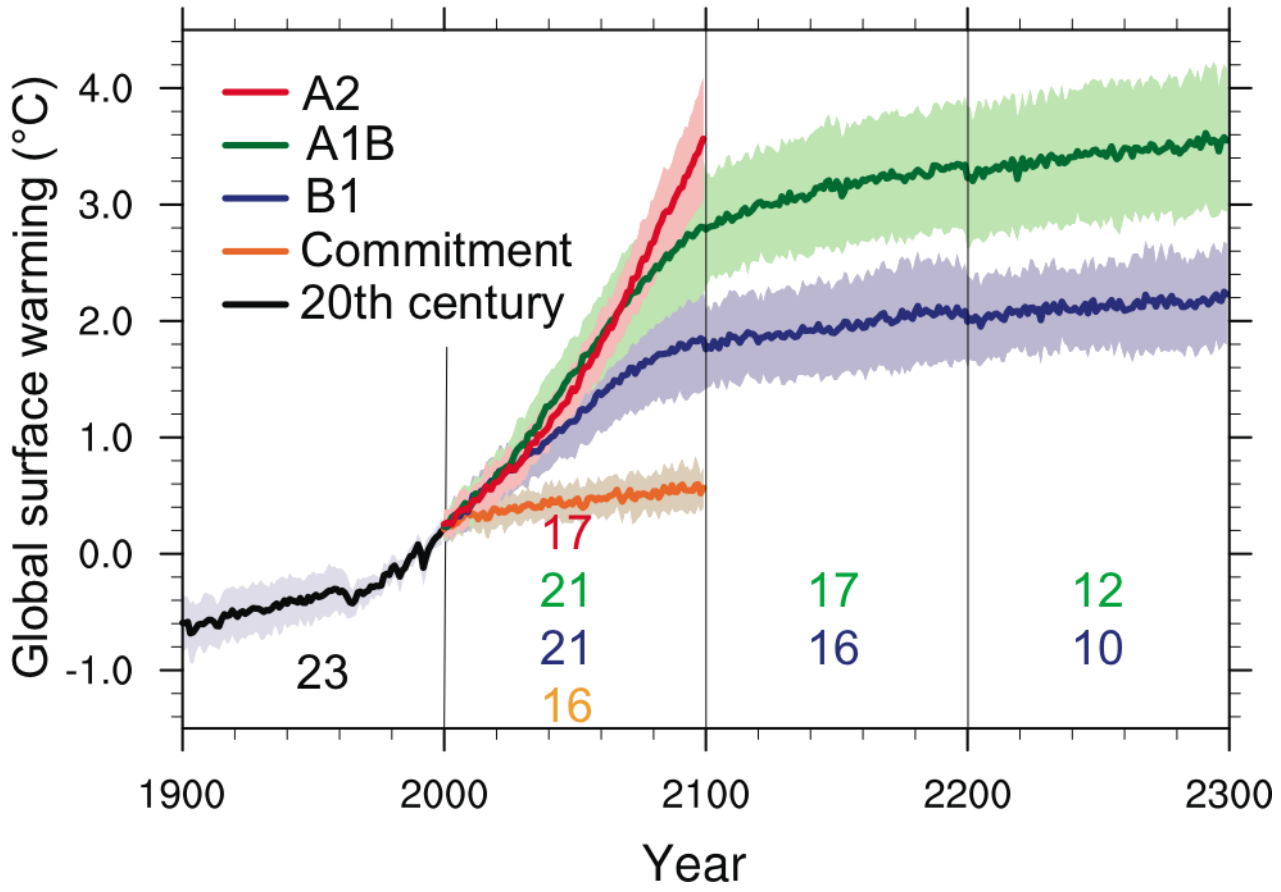

Figure 10.3.1. Multi-model means of surface warming for the scenarios A2, A1B and B1, shown as continuations of the 20th century simulation. Values beyond 2100 are for the stabilization scenarios (see Section 10.7). Linear trends from the corresponding control runs have been removed from these time series. Lines show the multi model means, shading denotes the plus minus one standard deviation range. Discontinuities between different periods have no physical meaning and are caused by the fact that the number of models that have run a given scenario is different for each period and scenario, as indicated by the coloured numbers given for each phase and scenario at the bottom of the panel. For the same reason, uncertainty across scenarios should not be interpreted from this figure (see Section 10.5 for uncertainty estimates).

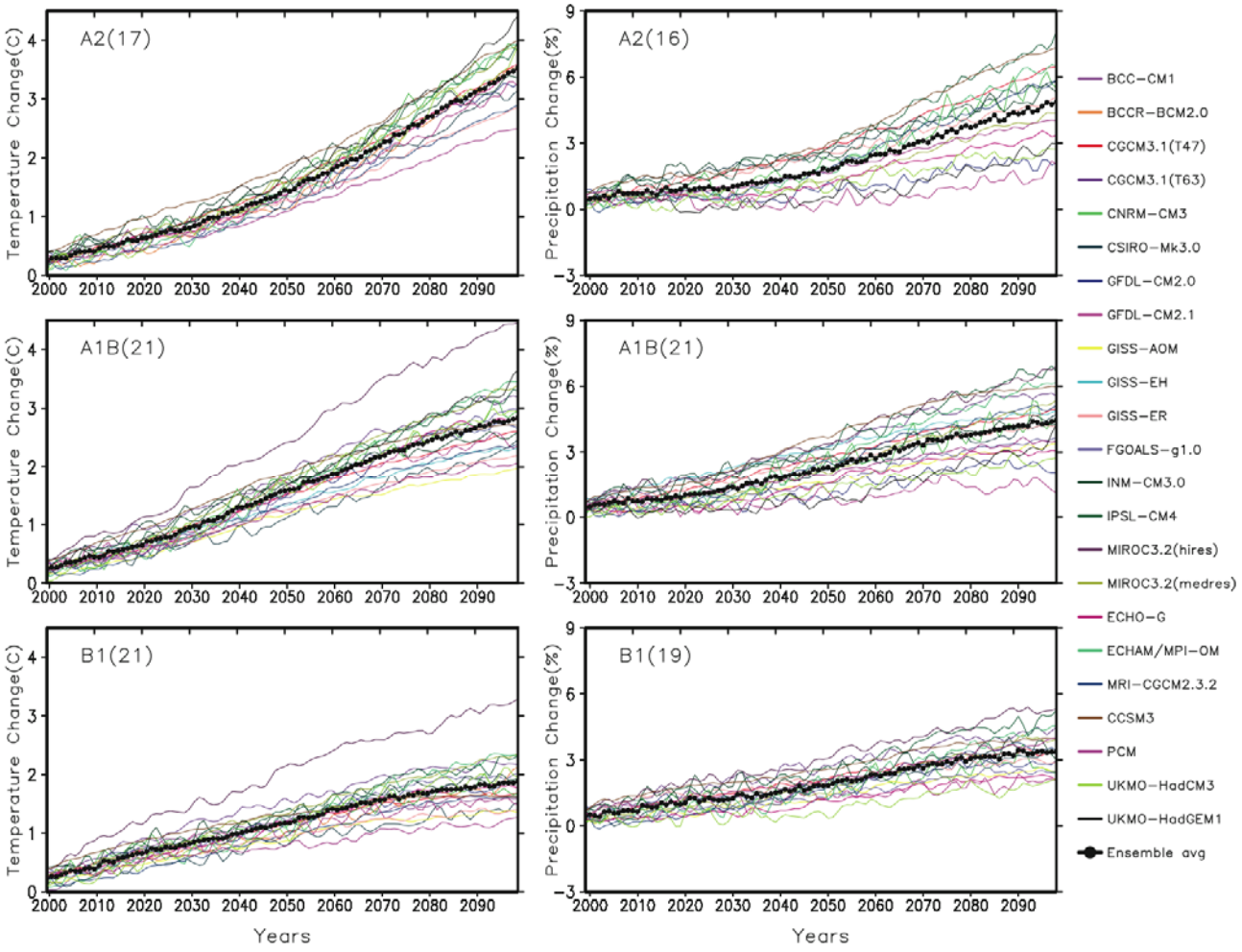

Figure 10.3.2. Time series of globally averaged (left) surface warming (surface air temperature change, in °C) and (right) precipitation change (in %) from the various global coupled models for the scenarios A2 (top), A1B (middle) and B1 (bottom). Values are annual means, relative to the 1980–1999 average from the corresponding 20th century simulations, with any linear trends in the corresponding control run simulations removed. Multi-model (ensemble) mean series are marked with black dots.

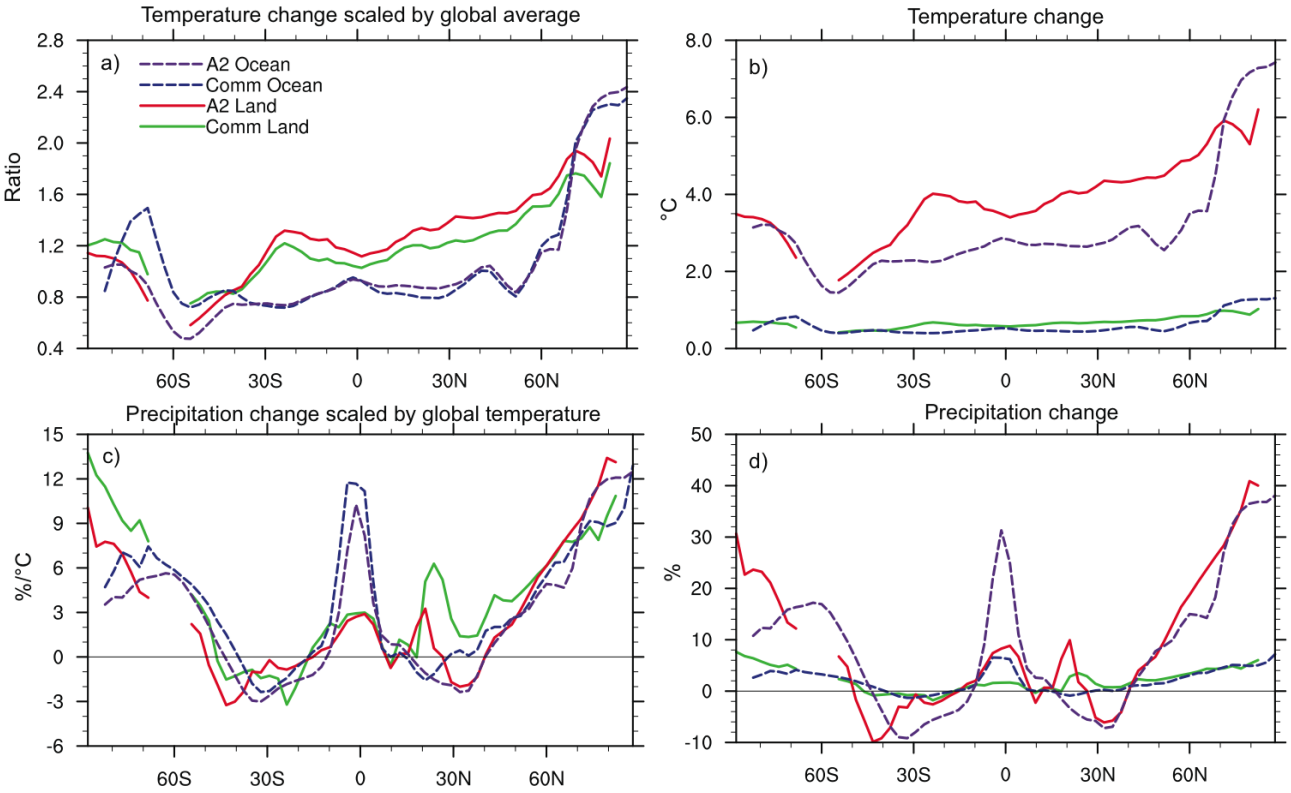

Figure 10.3.3. Zonal means taken over land and ocean separately, for annual mean surface warming (panels a and b) and precipitation (panels c and d), shown as a ratios scaled (a, c) and not scaled (b, d) with the global mean warming. Multi-model mean results are shown for two scenarios, A2 and Commitment (see Section 10.7), for the period 2080–2099 relative to 1980–1999. Results for individual models can be seen in supplementary material for this chapter.

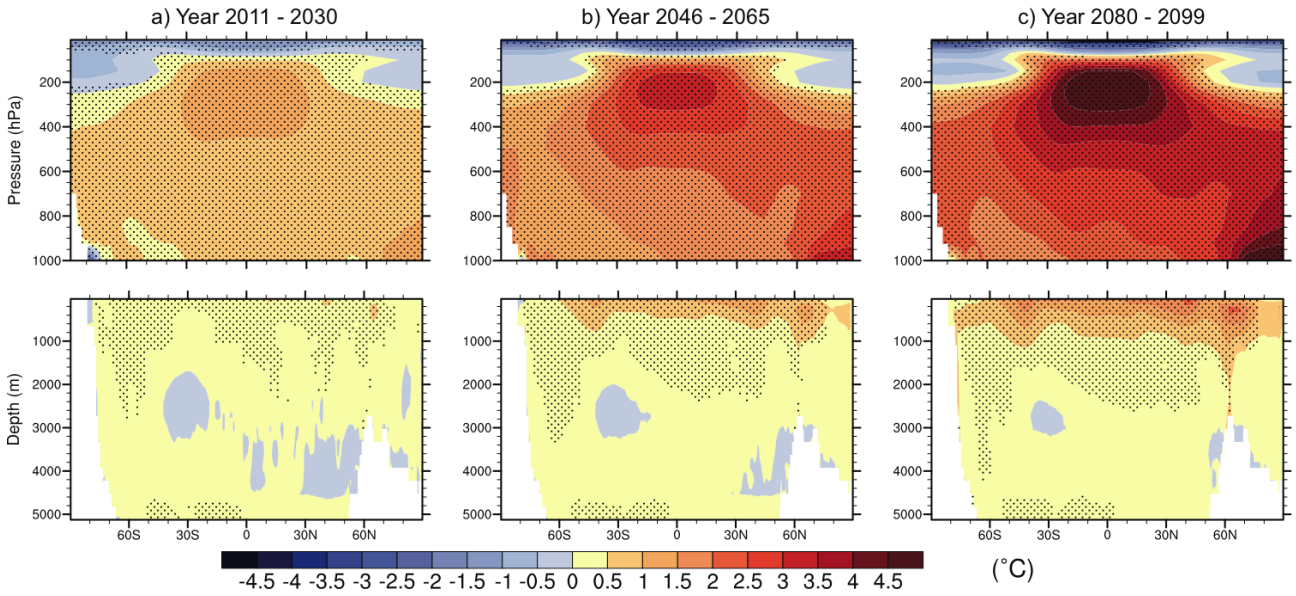

Figure 10.3.4. Zonal means of change in atmospheric and oceanic temperatures, shown as cross sections. Values are the multi-model means for the A1B scenario for three periods (a-c). Stippling denotes regions where the multi-model ensemble mean divided by the multi-model standard deviation exceeds 1.0 (in magnitude). Anomalies are given relative to the average of the period 1980–1999. Results for individual models can be seen in supplementary material for this chapter.

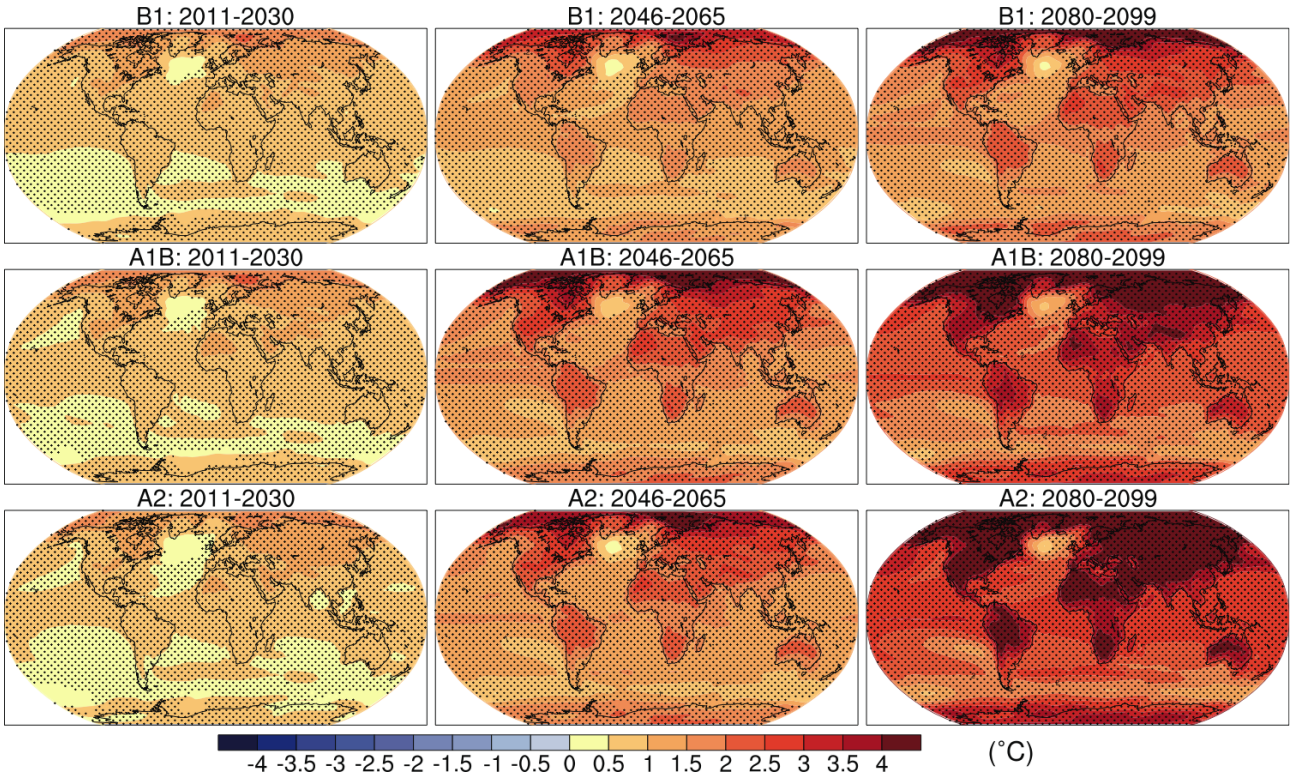

Figure 10.3.5. Multi-model mean of annual mean surface warming (surface air temperature change, in °C) for the scenarios B1 (top), A1B (middle) and A2 (bottom), and three time periods, 2011–2030 (left), 2046–2065 (middle), and 2080–2099 (right). Stippling denotes regions where the multi-model ensemble mean exceeds the intermodel standard deviation. Anomalies are given relative to the average of the period 1980–1999. Results for individual models can be seen in supplementary material for this chapter.

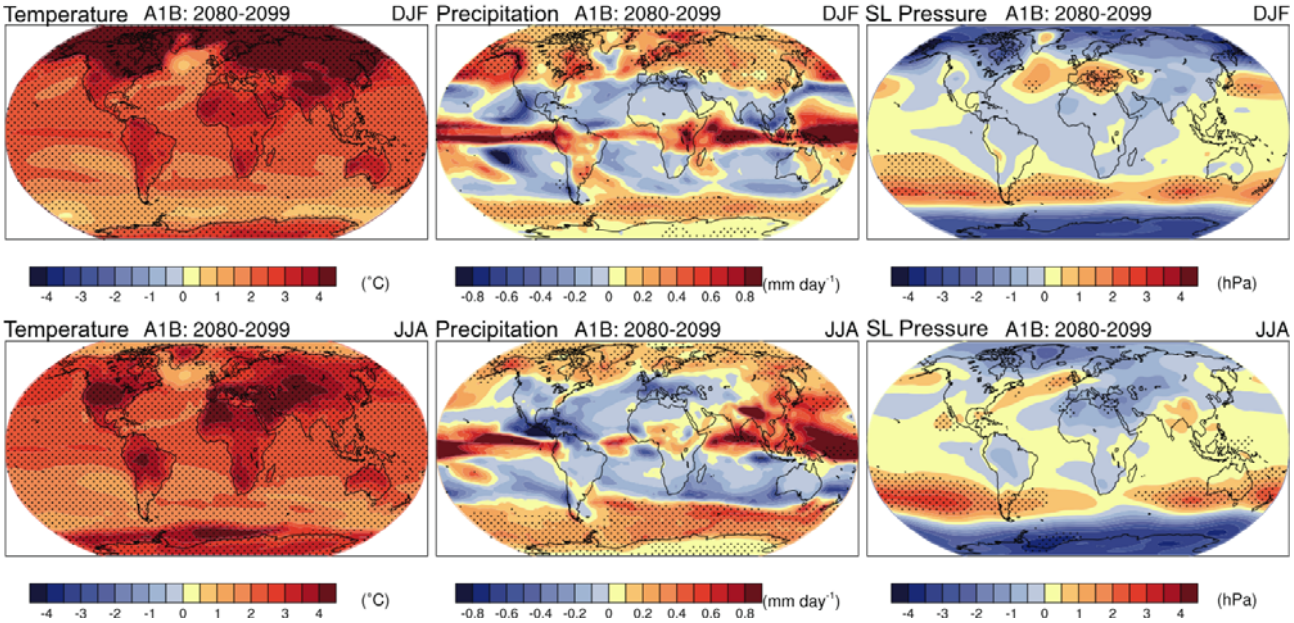

Figure 10.3.6. Multi-model mean changes of surface air temperature (°C, left), precipitation (mm/day, middle), and sea level pressure (hPa, right) for boreal winter (DJF, top) and summer (JJA, bottom). Changes are given for the scenarios SRES A1B, for the period 2080–2099 relative to 1980–1999. Stippling denotes areas where the magnitude of the multi-model ensemble mean exceeds the inter-model standard deviation. Results for individual models can be seen in supplementary material for this chapter.